Journal of Luminescence 131 (2011) 727–731

Contents lists available at ScienceDirect

Journal of Luminescence

journal homepage: www.elsevier.com/locate/jlumin

Biolabeling with nanoparticles based on Y_2O_3: Nd^{3+} and luminescence detection in the near-infrared

Cláudia A. Kodaira [a,1], Ana Valéria S. Lourenço [b,2], Maria Cláudia F.C. Felinto [a,1], Eduardo M.R. Sanchez [c,3], Francisco J.O. Rios [c,3], Luiz Antonio O. Nunes [d,4], Magnus Gidlund [c,3], Oscar L. Malta [e,5], Hermi F. Brito [b,*,2]

[a] Instituto de Pesquisas Energéticas e Nucleares, Av. Lineu Prestes 2242, 05508-000 São Paulo, Brazil
[b] Instituto de Química, Universidade de São Paulo, CP 26077, 05508-000 São Paulo, Brazil
[c] Departamento de Imunologia, Instituto de Ciências Biomédicas-IV, Universidade de São Paulo, Av. Lineu Prestes 1730,05508-900 São Paulo, Brazil
[d] Instituto de Física de São Carlos, Universidade de São Paulo, CP 369, 13660-970, São Carlos, Brazil
[e] Departamento de Química Fundamental, CCEN, Universidade Federal de Pernambuco Cidade Universitária, 50670-901 Recife, Brazil

ARTICLE INFO

Article history:
Received 3 August 2010
Received in revised form
26 October 2010
Accepted 22 November 2010
Available online 30 November 2010

Keywords:
Neodymium
Nanolabel
Luminescence
Immunoassay
Lipoprotein

ABSTRACT

Neodymium based fluorescence presents several advantages in comparison to conventional rare earth or enzyme–substrate based fluorescence emitting sources (e.g.Tb, HRP) . Based on this fact we have herein explored a Nd-based fluoroimmunoassay. We efficiently detected the presence of an oxidized low-density lipoprotein (oxLDL) in human plasma a well-known marker for cardiovascular diseases, which causes around 30% of deaths worldwide. Conventional fluoroimmunoassay uses time-resolved luminescence techniques, with detection in the visible range, to eliminate the fluorescence background from the biological specimens. By using an immunoassay based on functionalized Y_2O_3:Nd^{3+} nanoparticles, where the excitation and emission processes in the Nd^{3+} ion occur in the near-infrared (NIR) region, we have succeeded in eliminating the interferences from the biological fluorescence background, avoiding the use of time-resolved techniques. This yields higher emission intensity from the Nd^{3+}-nanolabels and efficient detection of anti-oxidized low-density lipoproteins (anti-oxLDL) by Y_2O_3:Nd^{3+}-antibody–antigen conjugation, leading to a novel biolabeling method.

1. Introduction

Atherosclerosis [1], the major mechanism behind cardiovascular disease, is the major cause of death in urban areas. Oxidative processes and dysplipidemias play a pivotal role in the evolution of the disease [2,3]. Following the quantification of oxidized low-density lipoprotein in plasma (oxLDL) has been shown to be a useful biomarker for the prevention and follow-up in patients. Even though quantitative (HPLC) or semi-quantitative assays exist, the latter show relatively low specificity and significant problems with background. Thus, the development of new clinical assays [4] for quantification of oxLDL in blood is required.

Rare earth ions (RE^{3+}) are excellent luminescent probes for biological systems because their narrow emission bands are easily recognizable and well separated, in the transient time scale, from the broad band fluorescence emissions from biological medium [5–7]. Applications in medical diagnostics make use of an immunoassay detected by time-resolved luminescence in order to allow the separation of the RE^{3+} ion luminescence from the fluorescence of the biological samples [8,9].

A number of important technological advances have been achieved applying nanotechnology for biomolecular detection using luminescent RE^{3+} nanomaterials [10–15]. Among the RE^{3+} ions, Eu^{3+} and Tb^{3+} are the most investigated, due to their intrinsic electronic spectroscopic properties in the visible region under excitation in the ultraviolet range [16]. Under this excitation, however, emissions arising from the metal ions, organic ligands and biological systems are typically present. In contrast, compounds containing Nd^{3+}, Er^{3+} and Yb^{3+} ions are relatively unexplored because these ions present weak luminescence intensity in the near-infrared (NIR) region [17–19]. This lack of research is mainly due to the technological advances in new detectors and excitation sources (e.g. lasers, LEDs, etc.), which have been developed only in the last decade.

Rare earth research on immunoassays has been almost exclusively on europium and terbium labeling using time-resolved luminescence techniques [20,21]. Phosphors with up-conversion characteristics are also applied in immunoassays and other biomedical analyses [6].

However, it would be highly desirable to be able to use RE^{3+} ions with emissions in the NIR region due to the reduction of interferences from the biological environment.

* Corresponding author. Tel.: +55 11 3091 3708; fax: +55 11 3091 3146.
E-mail address: hefbrito@iq.usp.br (H.F. Brito).
[1] Tel: +55 11 3133 9343; fax: +55 11 3133 9018.
[2] Tel: +55 11 3091 3708; fax: +55 11 3091 3146.
[3] Tel: +55 11 3091 7382; fax: +55 11 3091 7224.
[4] Tel: +55 16 3373 9835; fax: +55 16 3372 2218.
[5] Tel:+55 81 2126 7459; fax: +55 81 2126 8442.

0022-2313/$ - see front matter © 2010 Elsevier B.V. All rights reserved.
doi:10.1016/j.jlumin.2010.11.026

The main advantages of Nd^{3+} ion in immunoassays are: (i) it can be excited in the NIR region with lasers and LEDs, which do not induce electronic excitation in the biological medium; (ii) it presents high luminescence intensity at 1060 nm, where water molecules are transparent and (iii) it is not necessary to use time-resolved techniques to detect the luminescence that can be recorded at even extremely low Nd^{3+} concentrations.

The Nd^{3+} ion doped in a Y_2O_3 matrix [22] used in immunoassays can be beneficial, since it absorbs in both the visible and infrared regions (500–900 nm) with subsequent emission in the NIR region. Energy level diagram of the Nd^{3+} ion corresponding to absorbing levels may be excited using a laser pump at 808 nm, with emissions from the excited $^4F_{3/2}$ state to $^4I_{9/2}$ (890 nm), $^4I_{11/2}$ (1060 nm) and $^4I_{13/2}$ (1340 nm) manifolds. The $^4F_{3/2} \rightarrow {}^4I_{11/2}$ transition is of high technological interest and has been largely applied in the development of high power lasers. Our proposal is to use this high intensity emission in the area of immunoassays on the basis of the reasons given above. In addition, the Y_2O_3 matrix does not exhibit luminescence in the NIR region [22].

We report here a spectroscopic study of Y_2O_3:Nd^{3+} nanoparticles applied to fluoroimmunoassays. These nanomaterials were prepared by the combustion method [23]. The development of a new process to obtain silica particles incorporating Y_2O_3:Nd^{3+} with 3-aminopropyltrimethoxysilane (APTMS) used to provide the silica coating and the amino groups on the surface of the nanoparticles is also presented [24]. Furthermore, the covalent conjugation of these nanomaterials to the antibodies used in this new immunoassay is discussed.

2. Experimental

Y_2O_3:Nd^{3+} nanomaterials were prepared by the combustion method using glycine ($C_2H_5NO_2$) as fuel [23]. The starting materials for the synthesis of nanoparticles were $Y(NO_3)_3(H_2O)_6$, $Nd(NO_3)3(H_2O)_6$ (synthesized from Nd_2O_3—99.99%, Aldrich) and glycine (analytical grade, Merck). Aqueous stock solutions of Y^{3+} and Nd^{3+} nitrates were mixed in 0.5, 1, 2 and 5 mol% of Nd^{3+} with respect to Y^{3+} (precursor solutions). Three different glycine-to-nitrate ratios (G/N=1.0, 1.3 and 1.7) were employed to prepare nanoparticles containing Nd^{3+} as a dopant. The resulting homogeneous solutions were evaporated on a heater plate. When the excess of water was evaporated, spontaneous ignition occurred at around 300 °C, producing a fluffy solid that was grounded into a powder. The white powder sample was then heated at 600 °C for 10 h in order to decompose residual nitrate anions. The Y_2O_3:Nd^{3+} nanomaterials were functionalized using a microwave oven technique [24]. In this case, APTMS was added to the Y_2O_3:Nd^{3+} sample in order to encapsulate the luminescent nanoparticles. The mixture was sonicated for 5 min and then heated in the microwave oven for 1 min. This procedure was repeated until a homogeneous white mass was obtained. The resulting mass was heated at 150 °C for 30 min, ground to a powder, washed with distilled water and dried in a muffle at 70 °C. The use of APTMS in the functionalization step allowed the silica layer to protect the nanoparticles and provided amine groups on the particle surface to conjugate to the biological system. The ninhydrin method [25,26] was used to quantify the primary amine groups on the functionalized nanoparticles. A glycine solution was used for a standard calibration and the quantification of amine was made by measuring the absorbance at 570 nm against a reagent blank.

2.1. Fluoroimmunoassay using functionalized nanoparticles

The antibody used in this study has been described previously [27,28]. Monoclonal anti-oxLDL antibody was directly immobilized onto the amino-functionalized Y_2O_3:Nd^{3+} nanoparticles by the well established glutaraldehyde spacer method [29]. One milligram of the amino-functionalized particles was dispersed into a phosphate buffer solution (PBS: 0.05 mol L^{-1}, pH 7.4) containing 5% glutaraldehyde and stirred for 2 h. The solid particles were then washed four times with PBS, collected by centrifugation and conjugated to the anti-oxLDL antibody at different concentrations (0.25, 0.5, 1.0 and 2.5 μg mL^{-1}) at 4 °C for 12 h. Finally, the antibody-functionalized nanoparticles were washed four times with PBS solution in order to remove the excess antibody. The 96-well plate was coated with the oxLDL purified by ultracentrifugation at a concentration of 7.5 μg mL^{-1} in a carbonate–bicarbonate buffer (pH 9.6) overnight at 4 °C, as described in Refs. [3,30]. The wells were then washed four times with a PBS-T solution, containing 0.05 mol mL^{-1} PBS solution and 0.05% (v/v) Tween-20, blocked with gelatin 1% PBS-T and washed four times with PBS-T. The antibody-functionalized nanoparticles were then transferred to the 96-well plate. After 2 h at room temperature, the plate was washed four times with PBS-T and read. All fluoroimmunoassay data were executed simultaneously in triplicates.

2.2. Apparatus

X-ray diffraction patterns (XRD) of the samples were conducted using a Rigaku Miniflex and Cu-Kα radiation (30 kV and 15 mA) in the interval of 3–90° (2θ) with 1 s of pass time using the powder XRD method.

Transmission electron microscopy (TEM) images were recorded on a LEO 906E microscope operating at 80 kV. The samples were prepared by dispersing the fine powder with ethanol in an ultrasonic bath and then depositing a droplet of suspension on a copper microscope grid covered with porous carbon film.

Visible and near-infrared absorption spectra of the Y_2O_3:Nd^{3+} samples were recorded at room temperature on a Nicolet Magna 850 spectrophotometer in the spectral range of 550–1000 nm.

The luminescence spectra were measured at room temperature in the range of 800–1470 nm with excitation from a Ti–Sapphire laser pumped by an Ar laser model Innova 400 CR. The luminescence signals were filtered by a simple (0.3 m) monochromator, collected by an EG & G InGaAs detector and amplified by a lock-in. Excited state lifetime measurements were carried out using a Continuum OPO pumped by a Continuum Q-Switch Nd:YAG laser (10 ns). The resulting signal was recorded by an InGaAs detector and a Tektronix TDS380 digital oscilloscope.

3. Results and discussion

Y_2O_3:Nd^{3+} nanoparticles, prepared by the combustion method [23] using glycine (G) as a fuel and nitrate (N) as a precursor for G/N ratios equal to 1.0, 1.3 and 1.7, were characterized by X-ray diffraction (seen in Fig. S1). These nanomaterials presented characteristic diffraction pattern peaks of standard Y_2O_3 compounds with cubic structures, as defined by the Joint Committee for Powder Diffractions Standards (JCPDS card #25-1200). In addition, the average crystallite size, determined using Scherrer's formula, varied from 13 to 38 nm. It is interesting to note the increase in the crystallite size with increasing G/N ratio. The temperature of reaction also increased with the G/N ratio, achieving reaction at about 1000, 1320 and 1450 °C for 1.0, 1.3 and 1.7 G/N ratios, respectively, in agreement with the experimental results reported by Ye et al. [31].

Fig. 1 shows the transmission electron microscopy (TEM) image of the Y_2O_3:2%Nd^{3+} compound prepared by the combustion method for G/N=1.7. Generally, an agglomerate of particles was observed when the combustion method was employed. Based on

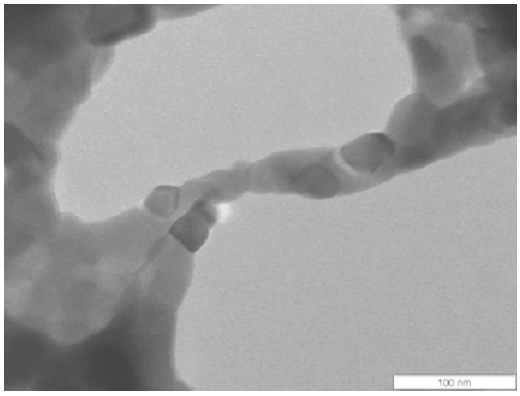

Fig. 1. TEM image of Y_2O_3:2%Nd^{3+} nanoparticles prepared by the combustion method.

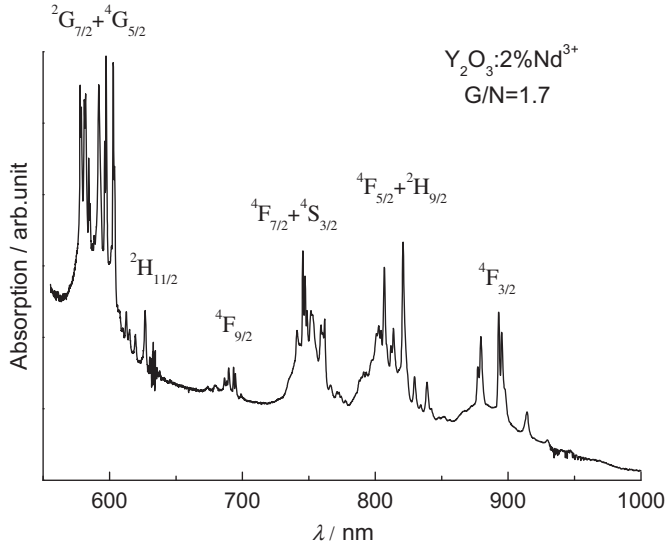

Fig. 2. Absorption spectrum of Y_2O_3:2%Nd^{3+} nanoparticles recorded at room temperature.

the TEM image (Fig. 1), the particle sizes varied from 25 to 40 nm, which agrees with those obtained from the X-ray diffraction pattern data (seen in Fig. S1).

The absorption spectrum of the Y_2O_3:2%Nd^{3+} nanoparticles ($G/N=1.7$) recorded at room temperature in the spectral range of 550–1000 nm is shown in Fig. 2. The narrow absorption bands of the Nd^{3+} ion were assigned to the $^4I_{9/2}\rightarrow{}^2G_{7/2}+{}^2G_{5/2}$ (579 and 597 nm), $^4I_{9/2}\rightarrow{}^2H_{11/2}$ (627 nm), $^4I_{9/2}\rightarrow{}^4F_{9/2}$ (689 nm), $^4I_{9/2}\rightarrow{}^4F_{7/2}+{}^4S_{3/2}$ (745 and 759 nm), $^4I_{9/2}\rightarrow{}^4F_{5/2}+{}^2H_{9/2}$ (805 and 821 nm) and $^4I_{9/2}\rightarrow{}^4F_{3/2}$ (893 nm) transitions [32]. Typical absorption transitions of the Y_2O_3:Nd^{3+} nanopowder were observed with similar spectral profiles to the absorption recorded for samples prepared by the ceramic method [22,33]. The Nd^{3+} ion has an odd-electron $4f^3$ configuration; therefore it was labeled as a Kramer ion due to its electronic states, which are at least doubly degenerate for any crystal field perturbation. The analyses of the energy levels of Y_2O_3:Nd^{3+} prepared by the ceramic method was reported by Gruber et al. [34]. As can be noted, the $^4I_{9/2}\rightarrow{}^2G_{7/2}$ and $^2G_{5/2}$ transitions (Fig. 2) split into 4 and 3 peaks, respectively, due to the crystal field interaction, indicating a non-cubic local symmetry around the Nd^{3+} ions.

The near-infrared emission spectra of Y_2O_3:2%Nd^{3+} nanopowders prepared by the combustion method at different glycine: nitrate ratios ($G/N=1.0$, 1.3 and 1.7) were recorded at 298 K from 800 to 1500 nm under excitation pump by a Ti–Sapphire laser at 808 nm (Fig. 3(a)). The luminescence spectra show the characteristic narrow bands assigned to 4f–4f transitions from the emitting $^4F_{3/2}$ level to the $^4I_{9/2}$, $^4I_{11/2}$ and $^4I_{13/2}$ levels, centered around 915, 1080 and 1350 nm, respectively (Fig. 3(a)). The $^4F_{3/2}\rightarrow{}^4I_{11/2}$ transition was seen to be the most prominent and was found in the "window of transparency" of water molecules, where water and biological tissues have minimal absorbance [17].

The luminescence data showed that the sample with the highest intensity had a neodymium concentration of 2% and a G/N ratio of 1.7 (Fig. 3(b) and (c)). Additionally, the lifetime values (τ) of the emitting $^4F_{3/2}$ level measured from the luminescence decay curves (seen in Fig. S2) of the Y_2O_3:Nd^{3+} samples with $G/N=1.7$ and 5.0%, 2.0%, 1.0% and 0.5% Nd^{3+} doping concentrations were 12, 70, 144 and 250 μs, respectively. It was noted that the τ values increased with decreasing dopant concentration, showing the luminescence concentration quenching effect associated with the non-radiative decay channel due to cross relaxation [35].

The Y_2O_3:2%Nd^{3+} material was then selected for application in the fluoroimmunoassay of LDL. In order to protect the nanoparticle from modification by acid and, at the same time, provide an amine terminal to allow conjugation to a proper ligand (e.g. biomolecules), the nanoparticles were capped with a silica layer containing amine groups by using microwave oven heating [24]. As such, APTMS was reacted with the nanoparticle surface, generating a

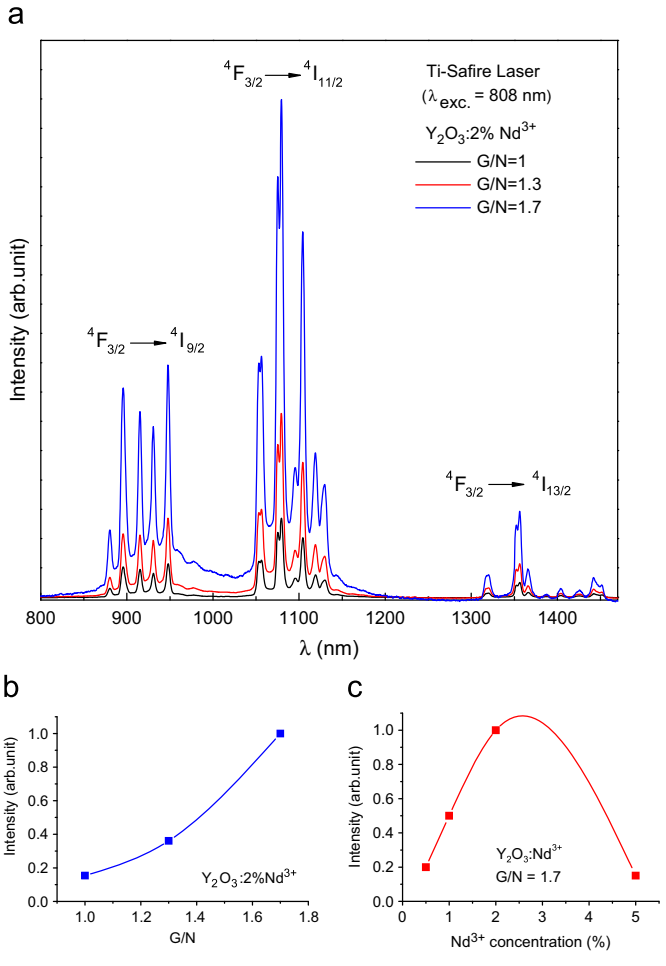

Fig. 3. (a) NIR emission spectra of Y_2O_3:2%Nd^{3+} samples prepared by the combustion method at different G/N ratios under excitation pump by a Ti–Sapphire laser at 808 nm and recorded at room temperature; (b) emission intensity as a function of Nd^{3+} doping concentration (%) and (c) emission intensity versus the G/N ratio.

covalent bonding between the silica layer and the Y_2O_3:Nd^{3+} particles.

The ninhydrin method [25,26] showed about 5780 nmol mg^{-1} of amine groups in the functionalized particles. After reaction with glutaraldehyde the nanoparticles showed only 250 nmol mg^{-1} of amine groups. This result demonstrated the existence of a high quantity of amine groups in the functionalized particles, and also that the reaction with glutaraldehyde was effective. The coupling between Ag–Ac and the nanoparticles was verified in the activity assay for immobilized enzyme horseradish peroxidase (HRP) [36,37], in order to prove the existence of molecular interactions between the antibody and nanoparticles (seen in SI). The functionalized Y_2O_3:2%Nd^{3+} nanoparticles were then established as a biological label in a homogeneous immunoassay (Fig. 4) for determining LDL.

Fig. 5 shows the integrated emission intensity of the $^4F_{3/2} \rightarrow {}^4I_{11/2}$ transition as a function of the concentration of functionalized nanoparticles bound to the LDL-antibody on the plate sensitized with oxLDL-antigen under excitation at 808 nm. Immunoassay responses were read in triplicate and a linear behavior (R=0.99987) was observed between the luminescence intensity and the labeled anti-oxLDL antibody concentration (mg $mL^{-1} \times 10^{-4}$), where the Nd^{3+} ion acts as the biological probe for optical detection of antibody. The inset in Fig. 5 shows the typical, narrow $^4F_{3/2} \rightarrow {}^4I_{11/2}$ emission of the Nd^{3+} ion in this biological luminescent probe.

It is important to emphasize that the neodymium biolabel allowed the detection of oxLDL on a nanometric scale (ng mL^{-1}), revealing the high efficiency of the process due to the high luminescence intensity and small sample requirement.

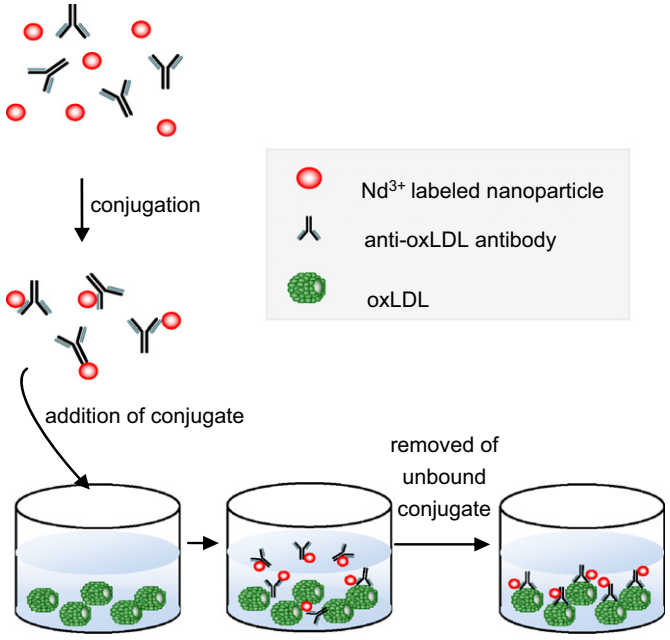

Fig. 4. Principle of fluoroimmunoassay for oxLDL detection based on the luminescence of Nd^{3+} nanoparticles.

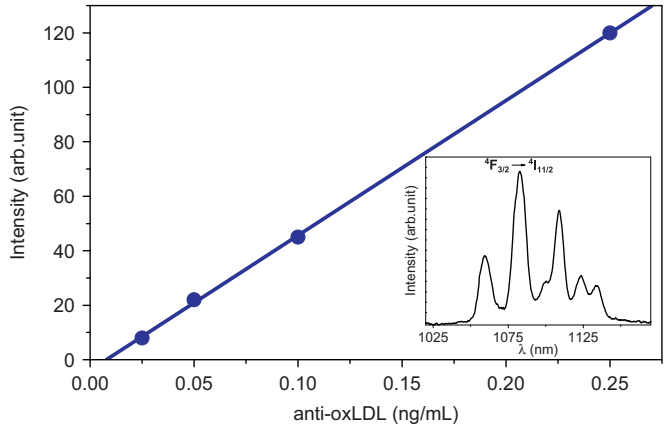

Fig. 5. Integrated emission intensity of the $^4F_{3/2} \rightarrow {}^4I_{11/2}$ transition as a function of functionalized nanoparticles bound to the anti-oxLDL antibody in the sensitized plate with oxLDL-antigen. The inset shows the emission spectrum obtained from the 96-well plate containing the anti-oxLDL labeled by the Y_2O_3:2%Nd^{3+} functionalized nanoparticles.

4. Conclusions

In this work we have reported a study on Y_2O_3:Nd^{3+} nanoparticles focusing on the great potential of this nanomaterial to be used in novel fluoroimmunoassays. As these nanoparticles display several advantages over other RE^{3+} based biolabels, their application in bioassays is certainly of interest. The functional integrity of these nanomaterials was maintained with 3-aminopropyltrimethoxysilane, which was used to provide the silica coating and the amine groups on the surface of the Y_2O_3:Nd^{3+} nanoparticles. Silica coating the surface of the nanoparticles helped to prevent their aggregation in water and improved their chemical stability, while the amino groups enabled the covalent conjugation to antibodies in a homogeneous immunoassay for oxidized low-density lipoprotein. Also of relevance was the fact that the Nd^{3+} material acted as a luminescent probe for oxLDL detection at concentrations on the nanomolar scale, revealing its high efficiency as a luminescent biomedical marker in the NIR region. In summary, a technological innovation for immunoassays based on functionalized Y_2O_3:Nd^{3+} nanoparticle as biolabel has been achieved that avoids interferences from biological background fluorescence.

Acknowledgements

This work was supported by FAPESP (Fundação de Amparo à Pesquisa do Estado de São Paulo) and CNPq (Conselho Nacional de Desenvolvimento Científico e Tecnológico). Additional support was provided by the RENAMI project (Brazilian Molecular and Interfaces Nanotechnology Network—CNPq) and inctINAMI (Brazilian Institute of Nanotechnology for Integrated Markers—CNPq).

Appendix A. Supplementary material

Supplementary material associated with this article can be found in the online version at doi:10.1016/j.jlumin.2010.11.026.

References

[1] T. Paul, K.U. Ingold, Angew. Chem. Int. Ed. 41 (2002) 804.
[2] A. Mertens, P. Holvoet, Faseb J. 15 (2001) 2073.
[3] D.F. Ketelhuth, G.C. Tonini, M.D.T. Carvalho, R.F. Ramos, P. Boschcov, M. Gidlund, Scand. J. Immunol. 68 (2008) 456.
[4] D.A. Giljohann, C.A. Mirkin, Nature 462 (2009) 461.
[5] J.-C.G. Bünzli, in: A. Sigel, H. Sigel (Eds.), Metal Ions in Biological Systems, Marcel Dekker Inc., New York, 2004, pp. 39–75.
[6] S.V. Eliseeva, J.-C.G. Bünzli, Chem. Soc. Rev. 39 (2010) 189.
[7] K. Binnemans, Chem. Rev. 109 (2009) 4283.
[8] J.-C.G. Bünzli, Chem. Lett. 38 (2009) 104.
[9] H. Siitari, I. Hemmilä, E. Soini, T. Lovgren, V. Koistinen, Nature 301 (1983) 258.
[10] D. Dosev, M. Nichkova, I.M. Kennedy, J. Nanosci. Nanotechnol. 8 (2008) 1052.
[11] C. Louis, R. Bazzi, C.A. Marquette, J.-L. Bridot, S. Roux, G. Ledoux, B. Mercier, L. Blum, P. Perriat, O. Tillement, Chem. Mater. 17 (2005) 1673.

[12] E. Beaurepaire, V. Buissette, M.-P. Sauviat, D. Giaume, K. Lahlil, A. Mercuri, D. Casanova, A. Huignard, J.-L. Martin, T. Gacoin, J.-P. Boilot, A. Alexandrou, Nano Lett. 4 (2004) 2079.
[13] N.C. Tansil, Z. Gao, Nanotoday 1 (2006) 28.
[14] G.K. Das, T.T.Y. Tan, J. Phys. Chem. C 112 (2008) 11211.
[15] M. Tan, G. Wang, Z. Ye, J. Yuan, J. Lumin. 117 (2006) 20.
[16] H.F. Brito, O.L. Malta, M.C.F.C. Felinto, E.E.S. Teotonio, in: J. Zabicky (Ed.), The Chemistry of Metal Enolate, John Wiley & Sons Ltd., England, 2009, pp. 131–184.
[17] M.D. Ward, Coord. Chem. Rev. 251 (2007) 1663.
[18] F.J. Steemers, W. Verboom, J.W. Hofstraat, F.A.J. Geurts, D.N. Reinhoudt, Tetrahedron Lett. 39 (1998) 7583.
[19] M.I. Gaiduk, V.V. Grigoryants, J. Photochem. Photobiol. B 7 (1990) 15.
[20] N. Hildebrandt, L.J. Charbonnière, M. Beck, R.F. Ziessel, H.-G. Löhmannsröben, Angew. Chem. Int. Ed. 44 (2005) 7612.
[21] H. Zhang, Y. Xu, W. Yang, Q. Li, Chem. Mater. 19 (2007) 5875.
[22] N.S. Prasad, W.C. Edwards, S.B. Trivedi, S.W. Kutcher, C.-C. Wang, J.-S. Kim, U. Hömmerich, V. Shukla, R. Sadangi, B.H. Kear, IEEE J. Sel. Top. Quantum Electron. 13 (2007) 831.
[23] C.A. Kodaira, R. Stefani, A.S. Maia, M.C.F.C. Felinto, H.F. Brito, J. Lumin. 127 (2007) 616.
[24] J. Feng, G. Shan, A. Maquieira, M.E. Koivunen, B. Guo, B.D. Hammock, I.M. Kennedy, Anal. Chem. 75 (2003) 5282.
[25] D. Shapilov, V.G. Kayumov, A.I. Krashenyuk, J. Anal. Chem. USSR 38 (1983) 436.
[26] I. Taylor, A.G. Howard, Anal. Chim. Acta 271 (1993) 77.
[27] M. Gidlund, N.R.T. Damasceno, J.A.L. Lindoso, D.S.P. Abdalla, H. Goto, Braz. J. Med. Biol. Res. 29 (1996) 1625.
[28] N.R.T. Damasceno, H. Goto, F.M.D. Rodrigues, C.T.S. Dias, F.S. Okawabata, D.S.P. Abdalla, M. Gidlund, J. Nutr. 130 (2000) 2641.
[29] W. Yang, C.G. Zhang, H.Y. Qu, H.H. Yang, J.G. Xu, Anal. Chim. Acta 503 (2004) 163.
[30] E.C. Fernvik, D.F.J. Ketelhuth, M. Russo, M. Gidlund, J. Clin. Immunol. 24 (2004) 170.
[31] T. Ye, Z. Guiwen, Z. Weiping, X. Shangda, Mater. Res. Bull. 32 (1997) 501.
[32] R. Bazzi, A. Brenier, P. Perriat, O. Tillement, J. Lumin. 113 (2005) 161.
[33] G.A. Kumar, J. Lu, A.A. Kaminskii, K.-I. Ueda, H. Yagi, T. Yanagitani, IEEE J. Quantum Electron. 42 (2006) 643.
[34] J.B. Gruber, D.K. Sardar, K.L. Nash, R.M. Yow, J. Appl. Phys. 102 (2007) 023103.
[35] G.A. Kumar, R.E. Riman, L.A. Diaz Torres, S. Banerjee, M.D. Romanelli, T.J. Emge, J.G. Brennan, Chem. Mater. 19 (2007) 2937.
[36] G.I. Berglund, Nature 417 (2002) 463.
[37] N.C. Veitch, Phytochemistry 65 (2004) 249.